

Toward experimental observations of induced Compton scattering by high-power laser facilities

Shuta J. Tanaka¹, Ryo Yamazaki^{1,2}, Yasuhiro Kuramitsu³, and Youichi Sakawa²

¹*Department of Physics and Mathematics, Aoyama Gakuin University, 5-10-1 Fuchinobe, Sagami-hara, Kanagawa 252-5258, Japan*

**E-mail: sjtanaka@phys.aoyama.ac.jp*

²*Institute of Laser Engineering, Osaka University, 2-6 Yamadaoka, Suita, Osaka 565-0871, Japan*

³*Graduate School of Engineering, Osaka University, 2-1 Yamadaoka, Suita, Osaka 565-0871, Japan*

.....
 Induced Compton scattering (ICS) is a nonlinear interaction between intense electromagnetic radiation and a rarefied plasma. Although the magnetosphere of pulsars is a potential site at which ICS occurs in nature, the ICS signatures have not been discovered so far. One of the reasons for non-detection of the ICS signatures is that we still do not attain the concrete understanding of such nonlinear plasma interactions because of their nonlinear nature and of the lack of experimental confirmations. Here, we propose a possible approach to understand ICS experimentally in laboratories, especially, with the use of the up-to-date short-pulse lasers. We find that the scattered light of ICS has characteristic signatures in the spectrum. The signatures will be observed in some current laser facilities. The characteristic spectrum is quantitatively predictable and we can diagnose the properties of the scattering plasma from the signatures.

Subject Index xxxx, xxx

1. Introduction

Pulsars — rotating neutron stars — are laser transmitters in nature. Their radio emission is coherent and their brightness temperature is so high, e.g., the Crab pulsar has record of 10^{37} K at 5.5 GHz [1]. The mechanism of the coherent radio emission is a long-standing mystery after the unexpected discovery of a neutron star in radio wavelength [2] and is a challenge from the nature to our knowledge of quantum and relativistic plasma physics [3]. Here, we discuss a potential to understand one of plasma processes in such an extreme condition experimentally by using up-to-date short-pulse lasers. The process which we study is known as induced Compton scattering (ICS).

ICS is a nonlinear interaction of strong electromagnetic waves and free electrons [4, 5], and is expected to occur around the pulsar magnetosphere [6]. As will be discussed in section 3, ICS studied in the present paper is different from another nonlinear interaction of strong electromagnetic wave and free electrons, named nonlinear Thomson (Compton) scattering (NTS) [7–12]. We have neither identified ICS signatures from pulsars nor in laboratories

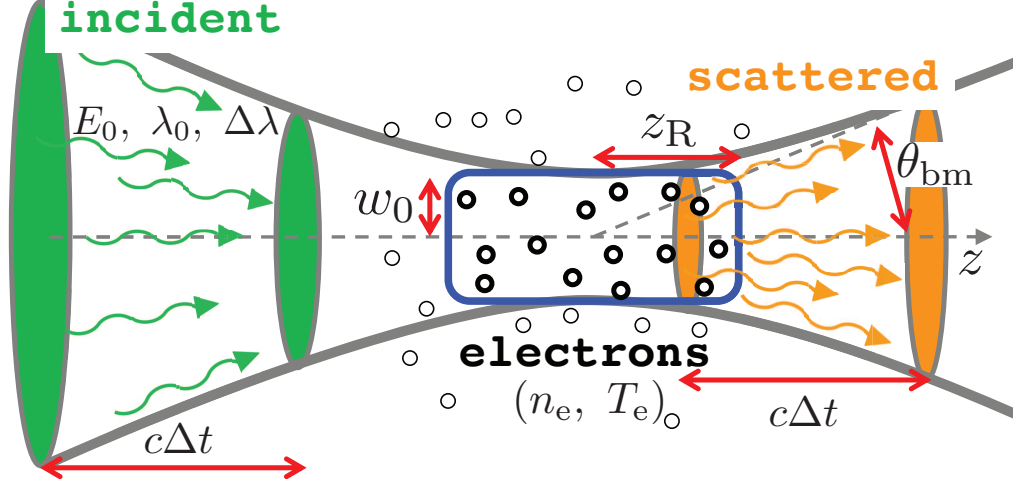


Fig. 1 Schematic picture of ICS in laboratory, i.e., an interaction between a Gaussian beam and electrons localized at the Rayleigh range (blue boxed region). The Rayleigh length z_R and the opening angle of the beam θ_{bm} are written in the laser parameters of the incident light (see text).

because we have not understood ICS quantitatively. Recently, one of the authors predicted that the scattered photon spectrum has characteristic line-like structures at red-side of the incident spectrum [13]. The spectral signature contains the information of the plasma, so that the better understanding of ICS would allow us to study the properties of the pulsar magnetosphere with the unprecedented way. Although their study assumed isotropic incident radiation field, we update their equation in order to apply laser radiation in laboratories, i.e., a directional narrow beam of an opening angle θ_{bm} depicted in Fig. 1.

The formulation of ICS is based on the Boltzmann-Uehling-Uhlenbeck equation which is the kinetic equation taking into account quantum corrections [14]. The laser radiation field is described by the occupation number, $n(\mathbf{r}, \mathbf{k})$, which is the photon number in a unit phase space volume $d^3\mathbf{r}d^3\mathbf{k}/(2\pi)^3$ at (\mathbf{r}, \mathbf{k}) . Laser radiation is usually described by a Gaussian beam, which is a solution of the paraxial Helmholtz equation deduced from the Maxwell's equations [15]. We have to relate $n(\mathbf{r}, \mathbf{k})$ with the five laser parameters: the total energy E_0 , the central wavelength (frequency) λ_0 (ν_0), the spectral (full-)bandwidth $\Delta\lambda$ ($\Delta\nu = c\Delta\lambda/\lambda_0^2$), the pulse width Δt and the minimum beam waist w_0 (Fig. 1). For simplicity, it is assumed that the incident radiation has the uniform directional distribution inside the solid angle $\Delta\Omega \approx \pi\theta_{bm}^2$ ($\theta_{bm} = \lambda_0/\pi w_0 \ll 1$) with a Gaussian spectrum, and that it is spatially uniform at the Rayleigh range $-z_R \leq z \leq z_R$ (blue boxed region in Fig. 1), i.e.,

$$n(z, \nu) \approx n_0 \exp\left(-2\frac{(\nu - \nu_0)^2}{\Delta\nu^2}\right), \quad 0 \leq \theta \leq \theta_{bm}. \quad (1)$$

The normalization constant n_0 relates to the laser parameters with the use of the definition of the total photon energy $E_0 \equiv \int g h \nu n(\mathbf{r}, \mathbf{k}) d^3\mathbf{r} d^3\mathbf{k} / (2\pi)^3$ as

$$n_0 \approx \frac{E_0}{h\nu_0 \Delta\nu \Delta t}, \quad (2)$$

where we used $d^3\mathbf{r} \approx \pi w_0^2 c \Delta t$, $d^3\mathbf{k}/(2\pi)^3 \approx \Delta\lambda\Delta\Omega/\lambda_0^4$, and the polarization degree of freedom $g = 1$. Because the brightness temperature of the radiation is $k_B T_b(\nu) = h\nu n(\nu)$, Eq. (2) corresponds to the Nyquist's relation. Note that T_b is constant along the ray and the opening angle decreases with the distance from the Rayleigh range. We set the opening angle is constant θ_{bm} in the Rayleigh range and consider ICS at the Rayleigh range.

We consider ICS off laser radiation by free electrons of density n_e and temperature T_e localized at the Rayleigh range at which the occupation number $n(\nu)$ is spatially uniform. In the low-temperature $\Theta \equiv k_B T_e/m_e c^2 \ll 1$ and low-frequency $\lambda_e/\lambda \equiv h\nu/m_e c^2 \ll 1$ limits, the kinetic equation for photons becomes

$$\frac{\partial n}{\partial y} = \frac{\Theta \theta_{\text{bm}}^6}{16} n \left\{ (k_\Theta^2 + 1) \frac{\partial}{\partial x} x^2 n + x \frac{\partial^3}{\partial x^3} x^3 n \right\} - \frac{n}{\Theta}, \quad (3)$$

where $y \equiv n_e \sigma_T c t \Theta$ is the Compton y -parameter (characteristic time or length), σ_T is the Thomson cross section, $x \equiv h\nu/k_B T_e$ is a normalized photon frequency, and $k_\Theta^2 \equiv 3/(2\Theta\theta_{\text{bm}}^2) - 1 \gg 1$ is a characteristic spectral width (see below) [13]. Eq. (3) is similar to the isotropic case [13] but has an explicit strong dependence on θ_{bm} . The first-derivative term in the right-hand side of Eq. (3) is the ‘‘ICS term’’ which is nonlinear in $n(x)$ and first order in terms of $\lambda_e/\lambda (= \Theta x \propto xy)$ and is corresponding to the quantum electron recoil effect boosted by the induced effect of bosons. The third-derivative term, which we call the ‘‘Doppler term’’, is also nonlinear in $n(x)$ and is second-order in terms of $\Theta\lambda_e/\lambda (= \Theta^2 x \propto xy\Theta)$ but plays a crucial rule in order to avoid unphysical multi-valued solutions by the Doppler effect [13]. The remaining term represents Thomson scattering, i.e., zeroth-order spontaneous scattering ($\propto y/\Theta$), and then the higher-order spontaneous scattering effects can be neglected.

The optical depth is given by $\tau \equiv \partial \ln n / \partial \ln y$, e.g., Thomson scattering has the well-known form $\tau_{\text{Th}} \equiv y/\Theta = n_e \sigma_T l$, where the scattering length $l = ct$ is set to $2z_R = 2\pi w_0^2/\lambda_0$. The optical depth to the ICS term is boosted by a factor of $\tau_{\text{ICS}}/\tau_{\text{Th}} \equiv (3/32)\theta_{\text{bm}}^4 k_B T_b/m_e c^2$ and has a strong dependence on θ_{bm} . In terms of the laser parameters, we have

$$\frac{\tau_{\text{ICS}}}{n_e} = \frac{3\sigma_T}{16\pi^3} \frac{E_0}{\Delta t \Delta \nu m_e c^2} \frac{\lambda_0^3}{w_0^2}. \quad (4)$$

Finally, the optical depth to the Doppler term is $\tau_D/\tau_{\text{Th}} \equiv (\Theta/16)\theta_{\text{bm}}^6 k_B T_b/m_e c^2$. The dispersive effect due to the third-derivative is the direct outcome of the Doppler term and then the ICS signatures will be observed for $\tau_{\text{ICS}} \gtrsim 0.1 \gg \tau_D > \tau_{\text{Th}}$ (Fig. 2). Typical values for some laser facilities are tabulated in Table 1.

2. Results

Fig. 2 shows numerical solutions to Eq. (3) applying the laser parameters of J-KAREN-P (top) and of NCU100TW (bottom-left). For example, in the top panel of Fig. 2, we show the dependence on τ_{ICS} so that $T_e = 200$ eV is common while $n_e = 10^{15} \text{ cm}^{-3}$ ($\tau_{\text{ICS}} \approx 0.09$) for thick-red and $n_e = 10^{16} \text{ cm}^{-3}$ ($\tau_{\text{ICS}} \approx 0.9$) for dashed-blue lines. The incident spectrum is a Gaussian (dotted-black line). Note that the scattered spectrum is almost identical to the incident one for $\tau_{\text{ICS}} \leq 0.01$. As seen in the isotropic case [13], the scattered spectrum shows the line-like features in red-side of λ_0 and their width is predictable from the steady-state

solution to Eq. (3),

$$x^2 \bar{n}(x) = A \cos(k_\Theta \ln x + \phi) + B + \frac{32}{3\Theta \theta_{\text{bm}}^4} x, \quad (5)$$

where an amplitude A , a DC component B , and a phase ϕ are constants of integration. The first term in the right-hand side of Eq. (5) shows that characteristic spectral full-width is logarithmic, i.e., $\delta x/x = \delta \lambda/\lambda \approx \pi/k_\Theta$, which is about θ_{bm} times narrower than the isotropic case [13]. Taking $A = 0$, Eq. (5) becomes the steady-state solution without the Doppler (dispersive) term.

The spectra in Fig. 2 show the five characteristics still similar to the isotropic case [13]. (1) The line-like features are formed intermittently and shift to longer wavelengths for larger n_e (τ_{ICS}), i.e., photons always lose their energy by ICS because of the electron recoil. (2) The line-like features have a characteristic logarithmic width of π/k_Θ . (3) The number of the line-like feature increases with n_e and decreases with T_e . (4) The separation between the line-like features increases toward longer wavelengths. (5) The intensity of the line-like features is higher at longer wavelengths. Although the number of photons are conserved for ICS, the total energy of scattered photons E_s is smaller than that of incident ones E_0 (bottom-right of Fig. 2).

Although τ_{ICS}/n_e (Table 1) of LFEX is larger than that of NCU100TW, we currently do not expect to observe the ICS signatures with the use of LFEX. This is because three additional conditions are imposed for the scattering electrons in order to observe the above five ICS signatures. We put four necessary conditions below, and Fig. 3 shows the allowed regions on the $n_e - T_e$ plane for given laser facilities. The present ICS experiment is suitable for high-power short-pulse lasers (J-KAREN-P and NCU100TW) rather than high-energy (long-pulse) lasers (LFEX).

Table 1 Parameters of the several laser facilities: “J-KAREN-P” at National Institute for Quantum and Radiological Science and Technology in Japan [16], “NCU100TW” at National Central University in Taiwan [17], and “LFEX” at osaka university in japan [18, 19].

Parameters	J-KAREN-P	NCU100TW	LFEX
E_0 [J]	10	3.3	400
λ_0 [nm]	820	810	1053
$\Delta\lambda$ [nm]	50	35	3.3
Δt [fs]	30	30	1500
w_0 [μm]	0.67	4.3	50
$k_{\text{B}} T_{\text{b}}/m_e c^2$	1.8×10^{14}	8.4×10^{13}	3.6×10^{15}
$\Delta\lambda/\lambda_0$	6.1×10^{-2}	4.3×10^{-2}	3.1×10^{-3}
θ_{bm}	3.9×10^{-1}	6.0×10^{-2}	1.3×10^{-2}
z_{R} [μm]	1.7	72	1.9×10^3
τ_{ICS}/n_e [cm^3]	9.0×10^{-17}	9.7×10^{-19}	2.7×10^{-18}
$\tau_{\text{D}}/(n_e \Theta)$ [cm^3]	9.0×10^{-18}	2.3×10^{-21}	3.3×10^{-22}
τ_{Th}/n_e [cm^3]	2.3×10^{-28}	9.5×10^{-27}	2.5×10^{-25}

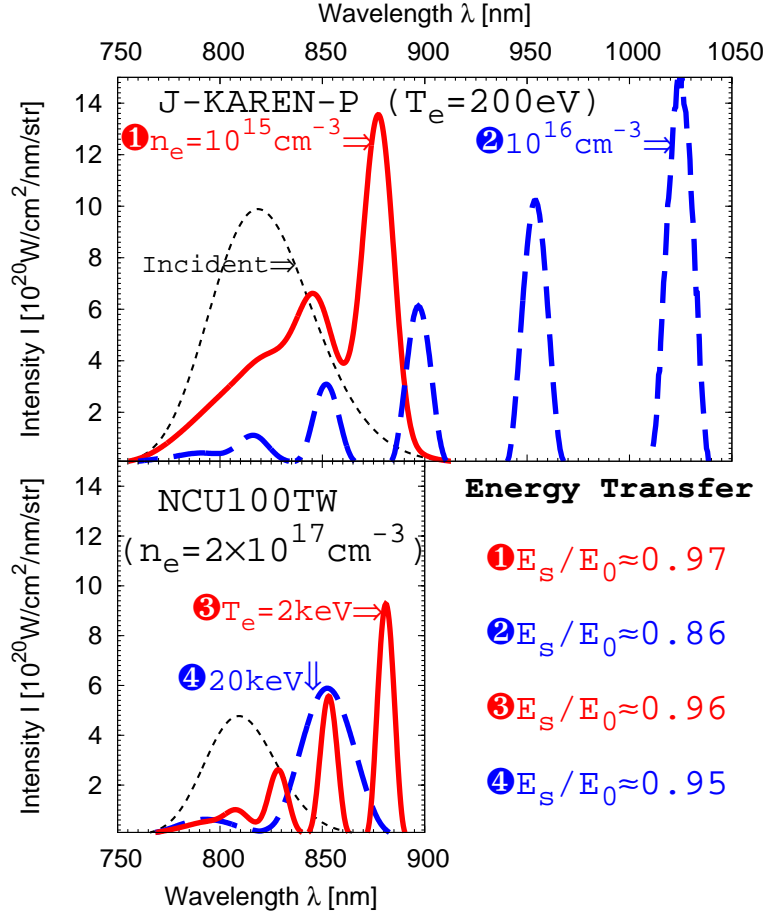


Fig. 2 Predicted spectra for laboratory experiments with J-KAREN-P (top) and by NCU100TW (bottom), where the dotted-black lines in both panels are the incident spectrum. (Top): $T_e = 200$ eV ($\Delta\lambda k_\Theta/\pi\lambda_0 \approx 3.1$) is common while the thick-red and dashed-blue lines are $n_e = 10^{15}$ cm $^{-3}$ ($(\tau_{ICS}, \tau_D, \tau_{Th}) \approx (0.09, 10^{-5.5}, 10^{-12.6})$) and 10^{16} cm $^{-3}$ ($(\tau_{ICS}, \tau_D, \tau_{Th}) \approx (0.9, 10^{-4.5}, 10^{-11.6})$), respectively. (Bottom-left): $n_e = 2 \times 10^{17}$ cm $^{-3}$ ($(\tau_{ICS}, \tau_{Th}) \approx (0.2, 10^{-10.0})$) is common while the thick-red and dashed-blue lines are $T_e = 2$ keV ($(\Delta\lambda k_\Theta/\pi\lambda_0, \tau_D) \approx (1.4, 10^{-7.0})$) and 20 keV ($(\Delta\lambda k_\Theta/\pi\lambda_0, \tau_D) \approx (4.5, 10^{-6.0})$), respectively. (Bottom-right): The ratios of the total photon energy before and after ICS E_s/E_0 are calculated for each case.

The first condition is $\tau_{ICS} > 0.1$ (dotted-green lines in Fig. 3) and gives a lower limit on n_e , such as

$$n_e > 1.1 \times 10^{15} \text{ cm}^{-3} \left(\frac{E_0}{10 \text{ J}} \right)^{-1} \left(\frac{\lambda_0}{820 \text{ nm}} \right)^{-5} \left(\frac{\Delta t}{30 \text{ fs}} \right) \left(\frac{\Delta\lambda}{50 \text{ nm}} \right) \left(\frac{w_0}{0.67 \mu\text{m}} \right)^2. \quad (6)$$

The second condition $\Delta\lambda/\lambda_0 > \pi/k_\Theta$ (dot-dashed-red) reduces an upper limit on T_e [13] and is written as

$$T_e < 31 \text{ keV} \left(\frac{\lambda_0}{820 \text{ nm}} \right)^{-2} \left(\frac{\Delta\lambda}{50 \text{ nm}} \right) \left(\frac{w_0}{0.67 \mu\text{m}} \right). \quad (7)$$

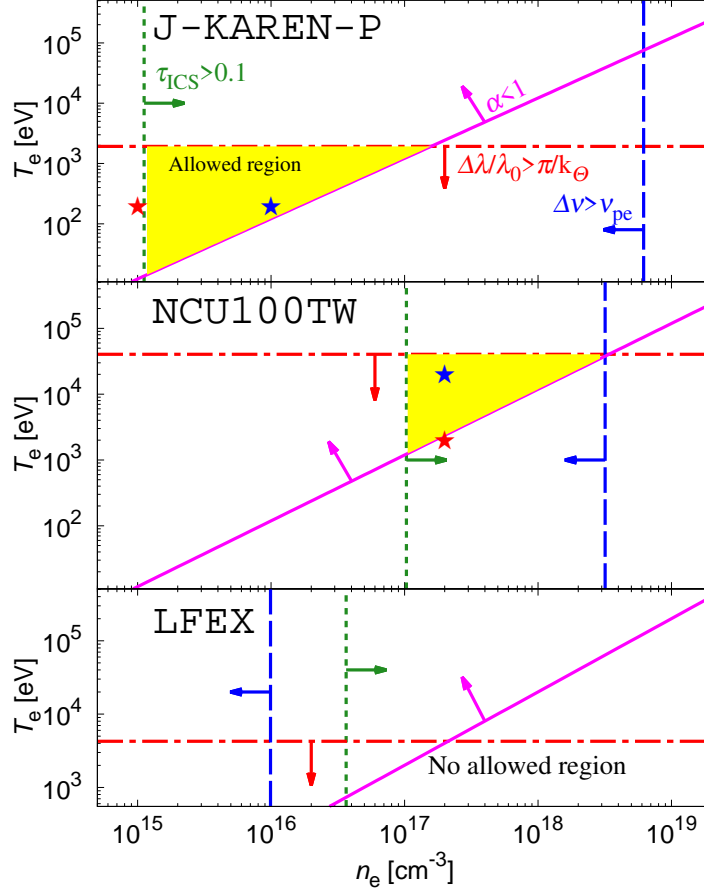


Fig. 3 Allowed regions (yellow marked) on the $n_e - T_e$ plane in order to observe the ICS signatures in each laser facility. We impose four necessary conditions (dotted-green, dot-dashed-red, dashed-blue and solid-magenta lines). The electron density should be large enough to deform the incident spectrum by ICS (Eq. (6)), while n_e should be small enough not to be contaminated by the plasma collective effects (Eqs. (7) and (9)). The electron temperature should be so small that the width of the line-like structure is smaller than the incident spectral width (Eq. (8)), while T_e should be large enough not to be contaminated by the plasma collective effects (Eq. (9)). Red and blue stars on the upper (J-KAREN-P) and middle (NCU100TW) panels are the parameters adopted in Fig. 2.

Note that the second condition is a practical requirement in order to observe the spectrum like Fig. 2 [13]. Although the interaction which violates only Eq. (7) is still ICS, its signatures will be different from those described above. The third (dashed-blue) and fourth (solid-magenta) conditions are requirements in order to dismiss the plasma collective effects. The higher-order Kompaneets equation (Eq. (3)) is valid when the spectral width $\Delta\nu$ are greater than the Langmuir plasma frequency $\nu_{pe} = \sqrt{n_e e^2 / \pi m_e}$ [20], which reads

$$n_e < 6.2 \times 10^{18} \text{ cm}^{-3} \left(\frac{\lambda_0}{820 \text{ nm}} \right)^{-4} \left(\frac{\Delta\lambda}{50 \text{ nm}} \right)^2. \quad (8)$$

Finally, we require the scattering parameter $\alpha \equiv \lambda_0/\lambda_{De}$ is less than unity in order to avoid the effects of the plasma screening, where $\lambda_{De} = \sqrt{k_B T_e/4\pi n_e e^2}$ is the Debye length [21], that is,

$$\frac{T_e}{n_e} > 1.2 \times 10^{-17} \text{ keV cm}^3 \left(\frac{\lambda_0}{820 \text{ nm}} \right)^2. \quad (9)$$

For high-energy (long-pulse) lasers such as LFEX, the condition of $\Delta\nu > \nu_e$ (dashed-blue) contradicts the condition of $\tau_{CS} > 0.1$ (dotted-green).

3. Discussion

There have been some attempts to observe ICS in laboratories in the last century [22–26]. Based on the qualitative arguments done at those times [27, 28], they reported some signatures of ICS. However, none of those facilities has the allowed parameter region on the $n_e - T_e$ plane as in the case of LFEX (bottom panel of Fig. 3) and then the phenomena which they found would be different from ‘ICS’ as we discussed in the present paper. In addition, our prediction is rather quantitative and peculiar so that the observed signature can be distinguished from the other nonlinear laser-plasma interactions.

ICS studied in the present paper is considered as the different physical process from NTS by the following three reasons. (1) ICS itself is the process preserving photon number [13], while NTS is not because, in the quantum view of NTS, multiple photons are absorbed by an electron and then the electron emits a single photon [8, 9]. (2) NTS is predominantly up-scattering process in contrast to ICS [7, 11] and (3) the scattering optical depths to ICS and NTS are not the same as follows. The (effective) cross section of NTS, i.e., the optical depth to NTS, is boosted by the square of the laser strength parameter compared with (linear) Thomson scattering, i.e., $\tau_{NTS}/\tau_{Th} \approx a_0^2$, where $a_0^2 \equiv (e\mathcal{E}\lambda_0/2\pi m_e c^2)^2 \propto \lambda_0^2 E_0/\Delta t w_0^2$ and \mathcal{E} is the amplitude of the electric field. Adopting the expression of the NTS cross section in classical limit from eq. (4.22) of [7], we have

$$\frac{\tau_{ICS}}{\tau_{NTS}} = \frac{3}{7\sqrt{2}\pi^2} \frac{\lambda_0^4}{r_e w_0^2 \Delta\lambda} \approx 2.2 \times 10^8 \left(\frac{\lambda_0}{820 \text{ nm}} \right)^4 \left(\frac{\Delta\lambda}{50 \text{ nm}} \right)^{-1} \left(\frac{w_0}{0.67 \text{ }\mu\text{m}} \right)^{-2}, \quad (10)$$

where the scattering length is also $l = 2z_R$ for NTS. Both ICS and NTS are clearly nonlinear processes because both τ_{CS} and τ_{NTS} are proportional to the laser radiation energy flux $E_0/\pi w_0^2 \Delta t$, however, they have different dependence on λ_0 , $\Delta\lambda$, and w_0 as seen in Eq. (10). They are distinct physical processes and are experimentally distinguishable.

Although ICS seems to always dominate over NTS from Eq. (10), previous experiments on NTS were not suitable for observing the signatures of ICS [10–12]. For the experiments using the relativistic electron beam [10, 12], Eq. (10) is modified by the relativistic Doppler effect. The strength parameter a_0 , i.e., τ_{NTS}/τ_{Th} , is an Lorentz invariant quantity but τ_{ICS}/τ_{Th} can be very small depending on the direction of the electron beam with respect to the laser radiation [6]. The experimental setup of [11] is rather similar to the present study but has no allowed region on the $n_e - T_e$ plane (Fig. 3) for their laser parameters, where $\Delta t \Delta\nu = 1$ is assumed for deducing the spectral width from their paper. In addition, NTS has an experimental advantage against ICS that is the spectral signatures of NTS, i.e., higher harmonics of the incident radiation [7–9], can be observed even for $\tau_{NTS} \ll 1$. For $\tau_{NTS} \ll 1$, the scattered radiation is dimmer about τ_{NTS} times than the (extremely bright) incident one

but still shows the higher harmonic spectrum as long as $a_0 \gtrsim 1$. For example, the observation of the second and third harmonics was made by [11] with the optical depth to NTS of $\tau_{\text{NTS,Chen98}} \sim 2z_{\text{R}}\sigma_{\text{T}}a_0^2n_{\text{e}} \approx 10^{-6}$ for their fiducial electron density of $n_{\text{e}} = 6.2 \times 10^{19} \text{ cm}^{-3}$. On the other hand, the spectral signatures of ICS, i.e, the line-like features of the similar intensity as the incident radiation (Fig. 2), do not appear for $\tau_{\text{ICS}} < 0.1$ at all (Eq. (6)). Although ICS far dominates over NTS in the present parameters (Eq. (10)), because a_0 of J-KAREN-P is as high as a hundred, we have chance to observe the signatures of NTS simultaneously with those of ICS (Fig. 2). The NTS signatures will be the l -th ($l \geq 2$) harmonics of the incident radiation ($\lambda_0/l = 410 \text{ nm}, 273 \text{ nm}, \dots$) and their intensity will be less than $\sim 10^{13} \text{ W cm}^{-2} \text{ nm}^{-1} \text{ str}^{-1}$, i.e., about τ_{NTS} times dimmer than the incident radiation.

Spectra of the scattered light of ICS inform us of the scattering electrons through n_{e} and T_{e} . An intriguing observational example in astrophysics is the giant radio pulses from the Crab pulsar. Although they basically have broad spectra [29], some show the spectral structure called ‘zebra band’ which is the line-like structures of $\Delta\nu/\nu \approx 0.06$ discovered from the Crab pulsar’s radio emission [30] and which can be a clue to understanding the physical condition of the pulsar magnetosphere. We need to extend the model including the relativistic and the strong magnetic field effects for the interpretation of the zebra band. Nevertheless, experimental confirmation of ICS in the present formulation is a step to understand the pulsar physics.

Alternative experiments can be done by the use of multiple beams. Strong dependence of ICS on θ_{bm} results from Eq. (1) in which we consider ICS at the Rayleigh range of one beam (Fig. 1). An extreme case would be the counter propagating beams which effectively increases the opening angle and ICS will be more effective than the present case. We leave the modeling of ICS in such a situation as a future study because even the isotropization of a directional electro-magnetic beam by ICS is under discussion [31–33]. ICS with LFEX will come under consideration for multiple beam experiments.

Finally, in the present treatment, we neglect back-reactions to plasma. The back-reactions do not only mean the plasma collective effects to scattered photons but also heating-up and/or acceleration of electrons by ICS [20]. In most of astrophysical situations, the radiation pressure force caused by electron scattering is evaluated by τ_{Th} as the Eddington luminosity [34]. However, the induced radiation pressure would be much stronger than the spontaneous one in this case [35]. Interestingly, τ_{ICS} increases with the laser power without increasing n_{e} so that individual electrons can easily attain to relativistic energy. For example of J-KAREN-P, the total number of electrons in the Rayleigh range volume is only $2\pi w_0^2 z_{\text{R}} n_{\text{e}} \approx 5 \times 10^3$ for $n_{\text{e}} = 10^{15} \text{ cm}^{-3}$. The total energy transferred to electrons is $E_0 - E_{\text{s}} \approx 0.3 \text{ J}$ and then each electron has 0.4 EeV on average. This mechanism can be possibly used for electron acceleration for the study of particle physics.

Acknowledgment

S.J.T. would like to thank Y. Ohira, H. Takabe, Y. Fukuda, F. Takahara and also the anonymous referee for useful discussions and helpful comments. This work is supported by JSPS Grants-in-Aid for Scientific Research Nos. 17H18270 (ST), 15H02154, 17H06202 (YS) and 18H01232 (RY), by Aoyama Gakuin University-Supported Program ‘‘Early Eagle Program’’ (ST), and also by the joint research project of the Institute of Laser Engineering,

Osaka University No. 2019B2-TANAKA (ST). R.Y. and S.J.T. deeply appreciate Aoyama Gakuin University Research Institute for helping our research by the fund.

References

- [1] T. H. Hankins, J. S. Kern, J. C. Weatherall, and J. A. Eilek, *Nature*, **422**, 141–143 (2003).
- [2] A. Hewish, S. J. Bell, J. D. H. Pilkington, P. F. Scott, and R. A. Collins, *Nature*, **217**, 709–713 (1968).
- [3] D. B. Melrose, *Rev. Mod. Phys.*, **1**, 5 (2017).
- [4] H. Dreicer, *Phys. Fluids*, **7**, 735–753 (1964).
- [5] Y. B. Zel’dovich, *Sov. Phys. Usp.*, **18**, 79–98 (1975).
- [6] S. J. Tanaka and F. Takahara, *Prog. Theor. Exp. Phys.*, **12**, 3 (2013).
- [7] E. S. Sarachik and G. T. Schappert, *Phys. Rev. D*, **1**(10), 2738–2752 (1970).
- [8] F. Mackenroth and A. di Piazza, *Phys. Rev. A*, **83**(3), 032106 (2011), arXiv:1010.6251.
- [9] D. Seipt and B. Kämpfer, *Phys. Rev. A*, **83**(2), 022101 (2011).
- [10] C. Bula, K. T. McDonald, E. J. Prebys, C. Bamber, S. Boege, T. Kotseroglou, A. C. Melissinos, D. D. Meyerhofer, W. Ragg, D. L. Burke, R. C. Field, G. Horton-Smith, A. C. Odian, J. E. Spencer, D. Walz, S. C. Berridge, W. M. Bugg, K. Shmakov, and A. W. Weidemann, *Phys. Rev. Lett.*, **76**(17), 3116–3119 (1996).
- [11] S.-y. Chen, A. Maksimchuk, and D. Umstadter, *Nature*, **396**(6712), 653–655 (1998).
- [12] W. Yan, C. Fruhling, G. Golovin, D. Haden, J. Luo, P. Zhang, B. Zhao, J. Zhang, C. Liu, M. Chen, S. Chen, S. Banerjee, and D. Umstadter, *Nature Photonics*, **11**(8), 514–520 (2017).
- [13] S. J. Tanaka, K. Asano, and T. Terasawa, *Prog. Theor. Exp. Phys.*, **2015**(7), 073E01 (2015).
- [14] E. A. Uehling and G. E. Uhlenbeck, *Phys. Rev.*, **43**, 552–561 (1933).
- [15] H. Kogelnik and T. Li, *Appl. Opt.*, **5**, 1550 (1966).
- [16] H. Kiriya, A. S. Pirozhkov, M. Nishiuchi, Y. Fukuda, K. Ogura, A. Sagisaka, Y. Miyasaka, M. Mori, H. Sakaki, N. P. Dover, K. Kondo, J. K. Koga, T. Z. Esirkepov, M. Kando, and K. Kondo, *Optics Letters*, **43**, 2595 (2018).
- [17] T.-S. Hung, C.-H. Yang, J. Wang, S.-y. Chen, J.-Y. Lin, and H.-h. Chu, *Applied Physics B: Lasers and Optics*, **117**, 1189–1200 (2014).
- [18] J. Kawanaka, N. Miyanaga, H. Azechi, T. Kanabe, T. Jitsuno, K. Kondo, Y. Fujimoto, N. Morio, S. Matsuo, Y. Kawakami, R. Mizoguchi, K. Tauchi, M. Yano, S. Kudo, and Y. Ogura, 3.1-kJ chirped-pulse power amplification in the LFEX laser, In *Journal of Physics Conference Series*, volume 112 of *Journal of Physics Conference Series*, page 032006 (2008).
- [19] Y. Arikawa, S. Kojima, A. Morace, S. Sakata, T. Gawa, Y. Taguchi, Y. Abe, Z. Zhang, X. Vaisseau, S. H. Lee, K. Matsuo, S. Tosaki, M. Hata, K. Kawabata, Y. Kawakami, M. Ishida, K. Tsuji, S. Matsuo, N. Morio, T. Kawasaki, S. Tokita, Y. Nakata, T. Jitsuno, N. Miyanaga, J. Kawanaka, H. Nagatomo, A. Yogo, M. Nakai, H. Nishimura, H. Shiraga, S. Fujioka, Firex Group, Lfex Group, H. Azechi, A. Sunahara, T. Johzaki, T. Ozaki, H. Sakagami, A. Sagisaka, K. Ogura, A. S. Pirozhkov, M. Nishikino, K. Kondo, S. Inoue, K. Teramoto, M. Hashida, and S. Sakabe, *Appl. Opt.*, **55**, 6850 (2016).
- [20] A. A. Galeev and R. A. Syunyaev, *Sov. Phys. JETP*, **36**, 669 (1973).
- [21] D. E. Evans and J. Katzenstein, *Reports on Progress in Physics*, **32**, 207–271 (1969).
- [22] I. K. Krasnyuk, P. P. Pashinin, and A. M. Prokhorov, *Sov. Phys. JETP*, **12**, 305 (1970).
- [23] M. Decroisette, J. Peyraud, and G. Piar, *Phys. Rev. A*, **5**, 1391–1396 (1972).
- [24] R. P. Drake, H. A. Baldis, R. L. Berger, W. L. Kruer, E. A. Williams, Kent Estabrook, T. W. Johnston, and P. E. Young, *Phys. Rev. Lett.*, **64**, 423–426 (1990).
- [25] W. P. Leemans, C. E. Clayton, K. A. Marsh, and C. Joshi, *Phys. Rev. Lett.*, **67**, 1434–1437 (1991).
- [26] M. J. Everett, A. Lal, D. Gordon, K. Wharton, C. E. Clayton, W. B. Mori, and C. Joshi, *Phys. Rev. Lett.*, **74**, 1355–1358 (1995).
- [27] J. Peyraud, *Journal de Physique*, **29**(1), 88–96 (1968).
- [28] J. F. Drake, P. K. Kaw, Y. C. Lee, G. Schmid, C. S. Liu, and M. N. Rosenbluth, *Phys. Fluids*, **17**, 778–785 (1974).
- [29] Ryo Mikami, Katsuaki Asano, Shuta J. Tanaka, Shota Kisaka, Mamoru Sekido, Kazuhiro Takefuji, Hiroshi Takeuchi, Hiroaki Misawa, Fuminori Tsuchiya, Hajime Kita, Yoshinori Yonekura, and Toshio Terasawa, *Astrophys. J.*, **832**(2), 212 (2016), arXiv:1608.07673.
- [30] T. H. Hankins and J. A. Eilek, *Astrophys. J.*, **670**, 693–701 (2007).
- [31] V. Y. Gol’Din, R. A. Syunyaev, and B. N. Chetverushkin, *Sov. Phys. JETP*, **41**, 18 (1975).
- [32] Y. B. Zel’dovich and R. A. Syunyaev, *Sov. Phys. JETP*, **41**, 391 (1975).
- [33] Y. E. Lyubarskii and S. A. Petrova, *Astron. Lett.*, **22**, 399–408 (1996).
- [34] A. S. Eddington, *Mon. Not. R. Astron. Soc.*, **77**, 16–35 (1916).
- [35] E. V. Levich, *Sov. Phys. JETP*, **34**, 59 (1972).